

Anelasticity to plasticity transition in a model two-dimensional amorphous solid

Baoshuang Shang(尚宝双)
Citation: Chin. Phys. B, 2024, 33 (**1**): 016102. DOI: 10.1088/1674-1056/acf82c
Journal homepage: http://cpb.iphy.ac.cn; http://iopscience.iop.org/cpb

What follows is a list of articles you may be interested in

Classification and structural characteristics of amorphous materials based on interpretable deep learning

Jiamei Cui(崔佳梅), Yunjie Li(李韵洁), Cai Zhao(赵偲), and Wen Zheng(郑文)
Chin. Phys. B, 2023, 32 (**9**): 096101. DOI: 10.1088/1674-1056/acd7d0

Enhanced mechanical and thermal properties of two-dimensional SiC and GeC with temperature and size dependence

Lei Huang(黄磊), Kai Ren(任凯), Huanping Zhang(张焕萍), and Huasong Qin(覃华松)
Chin. Phys. B, 2023, 32 (**7**): 076103. DOI: 10.1088/1674-1056/acc78f

Evolution of defects and deformation mechanisms in different tensile directions of solidified lamellar Ti-Al alloy

Yutao Liu(刘玉涛), Tinghong Gao(高廷红), Yue Gao(高越), Lianxin Li(李连欣), Min Tan(谭敏), Quan Xie(谢泉), Qian Chen(陈茜), Zean Tian(田泽安), Yongchao Liang(梁永超), and Bei Wang(王蓓)
Chin. Phys. B, 2022, 31 (**4**): 046105. DOI: 10.1088/1674-1056/ac1f0b

Mechanical property and deformation mechanism of gold nanowire with non-uniform distribution of twinned boundaries: A molecular dynamics simulation study

Qi-Xin Xiao(肖启鑫), Zhao-Yang Hou(侯兆阳), Chang Li(李昌), and Yuan Niu(牛媛)
Chin. Phys. B, 2021, 30 (**5**): 056101. DOI: 10.1088/1674-1056/abd162

Effect of nickel segregation on CuΣ9 grain boundary undergone shear deformations

Xiang-Yue Liu(刘湘月), Hong Zhang(张红), Xin-Lu Cheng(程新路)
Chin. Phys. B, 2018, 27 (**6**): 063103. DOI: 10.1088/1674-1056/27/6/063103

SPECIAL TOPIC — States and new effects in nonequilibrium

Anelasticity to plasticity transition in a model two-dimensional amorphous solid

Baoshuang Shang(尚宝双)[†]

Songshan Lake Materials Laboratory, Dongguan 523808, *China*

(Received 5 July 2023; revised manuscript received 17 August 2023; accepted manuscript online 9 September 2023)

Anelasticity, as an intrinsic property of amorphous solids, plays a significant role in understanding their relaxation and deformation mechanism. However, due to the lack of long-range order in amorphous solids, the structural origin of anelasticity and its distinction from plasticity remain elusive. In this work, using frozen matrix method, we study the transition from anelasticity to plasticity in a two-dimensional model glass. Three distinct mechanical behaviors, namely, elasticity, anelasticity, and plasticity, are identified with control parameters in the amorphous solid. Through the study of finite size effects on these mechanical behaviors, it is revealed that anelasticity can be distinguished from plasticity. Anelasticity serves as an intrinsic bridge connecting the elasticity and plasticity of amorphous solids. Additionally, it is observed that anelastic events are localized, while plastic events are subextensive. The transition from anelasticity to plasticity is found to resemble the entanglement of long-range interactions between element excitations. This study sheds light on the fundamental nature of anelasticity as a key property of element excitations in amorphous solids.

Keywords: amorphous solid, deformation mechanism, anelasticity to plasticity transition, molecular dynamics simulation

PACS: 61.43.–j, 62.40.+i, 71.55.Jv **DOI:** 10.1088/1674-1056/acf82c

1. Introduction

Amorphous solids, as non-equilibrium materials, have captivated the interest of both academic researchers and industrial applications due to their diverse deformation behaviors.[1–3] However, unlike crystalline materials, the underlying deformation mechanism in amorphous solids remains a topic of debate. While crystalline materials exhibit topological defects such as dislocations or grain boundaries as plasticity carriers, amorphous solids rely on shear transformations or rearrangement events rather than specific topological structures.[4–6]

Previous studies[7–11] have observed that rearrangement events in amorphous solids are localized and can occur within the apparent elastic regime. However, considering plastic rearrangements as excitation elements is inappropriate due to their entanglement with long-range elastic interactions and plastic events.[12–18] Consequently, identifying the excitation element in amorphous solids remains a topic of ongoing debate.[5,19]

Furthermore, it is crucial to note that not all rearrangement events in amorphous solids exhibit irreversible plastic behavior. Recently, a new type of rearrangement event characterized by an intrinsic anelastic nature has garnered significant attention.[20–23] Unlike plastic events, these anelastic rearrangements are reversible during the loading–unloading process. They play a vital role in influencing various mechanical properties of amorphous solids, including relaxation,[24,25] thermal cycling rejuvenation,[26] mechanical anisotropy,[27,28] and memory effect.[29,30]

However, the understanding of the discrepancies and connections between anelastic and plastic events, as well as the key parameters governing the transition from anelasticity to plasticity, remains elusive. Further investigations are necessary to unravel the underlying mechanisms and establish a comprehensive understanding of the relationship between these two deformation modes in amorphous solids.

In this study, we aim to address these questions through molecular dynamics simulations. We investigate the mechanical response of amorphous solids using athermal quasistatic shear and frozen matrix methods. Our focus is on observing the transition from anelasticity to plasticity and understanding the underlying mechanisms. By analyzing the characterized parameters, we identify three distinct deformation modes: elasticity, anelasticity, and plasticity. Specifically, we explore the effects of finite system size on these parameters. Our findings reveal that anelasticity precedes plasticity and serves as a critical intermediary between elasticity and plasticity. Furthermore, we observe that anelastic events, characterized by their system size independence, exhibit a localized nature within the material. On the other hand, plastic events display subextensive behavior. This suggests that plasticity emerges from the collective interaction of a series of anelastic events. As a result, anelastic events can be regarded as potential element excitations in amorphous solids.

[†]Corresponding author. E-mail: shangbaoshuang@sslab.org.cn

© 2024 Chinese Physical Society and IOP Publishing Ltd

2. Method

2.1. Initial sample preparation

We used a well studied two-dimensional binary Lenard–Jones model with a polynomial cutoff smooth[21,31] to investigate the mechanical property of amorphous solid. All units were expressed in terms of the mass m and the two parameters describing the energy and length scales of interspecies interaction, ε and σ, and the Boltzmann constant $k_B = 1$. Therefore, the time was measured in units of $t_0 = \sqrt{m\sigma^2/\varepsilon}$, and the temperature was measured in units of $T_0 = \varepsilon/k_B$. The composition ratio of large (L) and small (S) was $N_L : N_S = (1+\sqrt{5})/4$. 100 samples each containing 10^4 atoms with periodic boundary condition were obtained by quenching from $T = 2.0$ to $T = 0.18$ with constant volume, and the quench rate was fixed at 0.0000325 T_0/t_0, and then the initial sample was obtained by minimized the quenched sample with conjugate gradient (CG) method, where the fictive temperature of the sample was around 0.335. The reduced density of system was fixed at 1.02. All the results were presented in reduced units. We performed all the simulations using the LAMMPS molecular dynamics package,[32] and used the OVITO package[35] for atomic visualization.

2.2. Frozen matrix method

Frozen matrix method is a useful tool to investigate the local yield stress[34] or local modulus[35] of the amorphous system, and local relaxation time[17] of supercooled liquid, it can also use to study the thermally activated rearrangement[36] and to calibrate more quantitatively elastoplastic models,[37] even for different preparation protocols.[38] Here, we extended this method to study the anelasticity to plasticity transition in the amorphous solid. The investigated region was selected within a radius R, then the outside region was frozen with affine deformation (Fig. 1(a)). In this study, the investigated region was fixed at the center of each sample. The mechanical response of amorphous solid was probed by the athermal quasi-static shear (AQS) protocol. The simple shear deformation was performed in all regions and the shear strain increment was $\delta\gamma = 10^{-5}$, during each shear strain increment, the investigated region was relaxed by energy minimization, and the outside region was frozen with affine deformation. The loading process continued until the shear strain reached 0.3. The choice of 0.3 was not grounded in specific physical reasoning; rather, it was selected to ensure that all investigated samples exhibited a transition from anelasticity to plasticity.

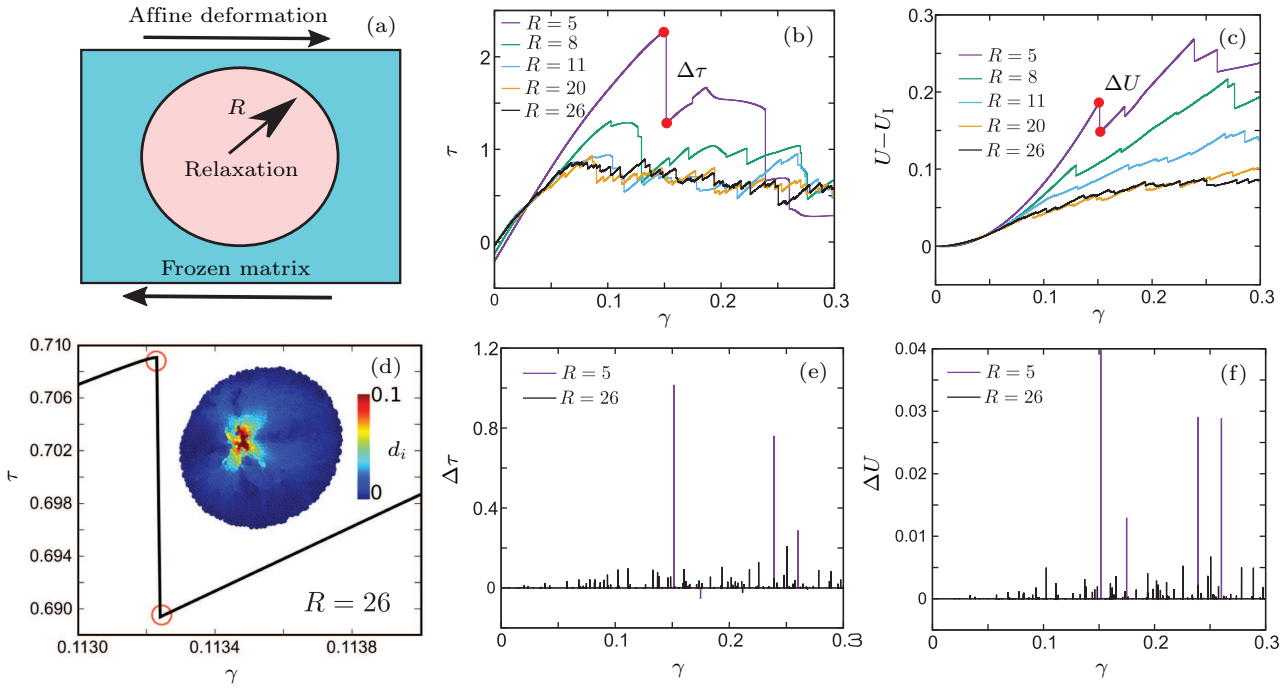


Fig. 1. The loading process of the amorphous solid. (a) The schematic of frozen matrix deformation. (b) The shear stress τ changes with shear strain γ in various systems. (c) The potential energy $U - U_I$ changes with strain in various systems. (d) The typical stress drops in $R = 26$ system and the corresponding atomic displacement color map shown in the inset. (e) The stress drops ($\Delta\tau$) changes with strain in $R = 5$ and $R = 26$ systems. (f) The potential energy drop (ΔU) changes with strain in $R = 5$ and $R = 26$ systems, respectively.

2.3. Physical property characterization

2.3.1. Anelastic event and plastic event

During the loading process, stress and potential energy drops occur (Figs. 1(b) and 1(c)), which are caused by rearrangement events (Fig. 1(d)). A rearrangement event is defined as when the maximum atomic displacement exceeds 0.1, or the potential energy drop per atom ΔU is greater than 0.1, in the investigated region. To characterize the anelastic and plastic events, the following unloading process was performed. After each potential energy drop, the shear strain was reversed and sheared back to $\gamma = 0$, which is called the unloaded sam-

ple. The mean squared displacement (MSD) between the unloaded sample and the initial sample was compared, and if MSD was zero, the drop was an anelastic event; otherwise, it was a plastic event. The potential energy per atom U and the shear stress τ of the investigated region were monitored during the loading and unloading processes, and the shear strain increment was fixed at $\delta\gamma = 10^{-5}$.

2.3.2. Atomic displacement

To compare configuration 1 and configuration 2, the atomic displacement of atom i is defined as $\boldsymbol{d}_i = \boldsymbol{r}_i(1) - \boldsymbol{r}_i(2)$, where $\boldsymbol{r}_i(1)$ is the coordination vector of atomic i at configuration 1. The MSD between two configurations can be defined as $1/N\sum_{i\in N}\boldsymbol{d}_i\cdot\boldsymbol{d}_i$, where N is the atomic number in the investigation region.

3. Results and discussion

Figure 1 shows the loading process of the amorphous solid with various system sizes. There are notable finite size effects with frozen matrix boundary condition, both the frequency of stress drop $\Delta\tau$ and potential energy drop per atom ΔU increase with system size R. Conversely, the amplitudes of $\Delta\tau$ and ΔU decrease with the system size (Figs. 1(e) and 1(f)). During the stress drop (Fig. 1(e)), the atomic displacement d_i shows a typical quadrupolar symmetry. This is qualitatively consistent with the situation with periodic boundary condition.[10,39] However, the frozen matrix boundary condition not only blocks the long range elastic interaction from outside region, but also causes significant confinement effect.[17] As suggested by Regev *et al.*,[23] the confinement effect can lead to reversible rearrangement. As shown in Fig. 2, for $R = 6$ system, both the stress and potential energy state are fully recovered after the loading–unloading process, indicating an anelastic behavior. In contrast, for $R = 26$ system, both the stress and potential energy states are different from the initial ones, indicating a plastic behavior. Interestingly, for $R = 11$ system, the stress state is almost recovered but the energy state is not. This behavior can be attributed to the confinement effect of the frozen matrix boundary, and it signifies a transition from anelasticity to plasticity controlled by the system size. Increasing the system size weakens the confinement effect, thereby influencing the nature of the deformation response.

Moreover, it should be noted that for a given system size, the increase in strain can also lead to a transition from anelasticity to plasticity. This behavior is depicted in Fig. 3, which illustrates the loading process with various unloading processes for a system size of $R = 11$. When the unloading process starts from a strain of $\gamma = 0.14$, the potential energy of the system can be fully recovered to its initial state. However, when the unloading process starts from $\gamma = 0.15$ or $\gamma = 0.19$, the potential energy of the unloaded samples (back-1 and back-2) is higher than that of the initial state (Fig. 3(a)). The loading process exhibits a characteristic first drop strain, denoted as $\gamma_e = 0.02545$ (Fig. 3(b)). When the loading strain γ is smaller than γ_e, the loading–unloading process can be fully recovered. This behavior is indicative of elasticity, where no dissipation ($\oint \tau \mathrm{d}\gamma \equiv 0$) occurs during the loading phase.

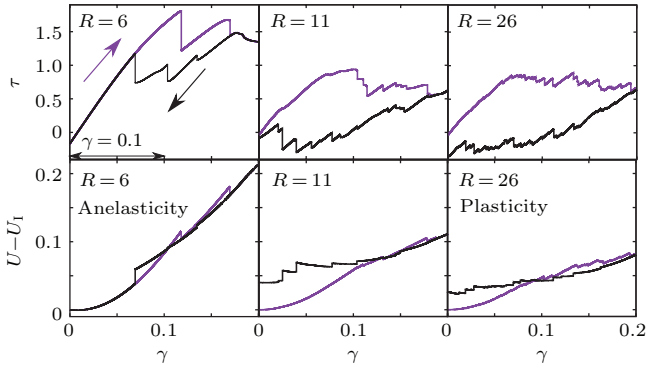


Fig. 2. The loading and unloading process for various system sizes. The up panel shows the shear stress evolves with shear strain during loading and unloading processes, the down panel shows the potential energy evolves with shear strain. The purple arrow and black arrow illustrate the loading and unloading directions, respectively.

In addition, when the loading strain exceeds γ_e ($\gamma > \gamma_e$), the potential energy–strain curve exhibits sudden drops, indicating atomic rearrangement events. These energy drops are further examined through the unloading process. The last energy drop corresponding to an anelastic event can be identified (Fig. 3(c)). The loading process exhibits a last anelastic drop strain denoted as $\gamma_p = 0.145$. For loading strains between γ_e and γ_p, the loading–unloading process can be fully recovered, but dissipation occurs. When the loading strain exceeds γ_p ($\gamma > \gamma_p$), the unloaded sample cannot be fully recovered to its initial state, and plastic rearrangement takes place. The displacement color map of the anelastic drop is presented in Fig. 3(d). A comparison of the atomic displacement during the anelastic drop with the plastic displacement of back-1 and back-2 samples reveals that the atomic displacement during the anelastic drop is reversible, while plastic rearrangement results in permanent displacement. By comparing the energy of the unloaded sample with that of the initial state, three types of mechanical properties during the loading process can be identified: elasticity, anelasticity, and plasticity (Fig. 3(e)).

The anelasticity to plasticity transition is both controlled by system size R and loading strain γ, and the key parameters for the transition are γ_e and γ_p. Figure 4(a) shows that the mean values of γ_e and γ_p decrease with system size R, and the finite size effect can be well depicted by a power-law formula $\gamma \sim R^{-\alpha}$, i.e., $\gamma_e \sim R^{-1.09\pm0.02}$ and $\gamma_p \sim R^{-0.86\pm0.04}$. The discrepancy of exponent between γ_e and γ_p reveals that, as the system size increases, the anelastic property will be more

significant. It will dominate the deformation of the apparent elastic region. Furthermore, for thermodynamic limit $R \to \infty$, both elasticity and anelasticity will disappear, and the intrinsic mechanical property of amorphous solid is inelasticity, this is consistent with the observation of avalanche statistics in the apparent elastic region.[17] It confirms that regardless of the boundary condition, the nature of amorphous solid is inelastic.

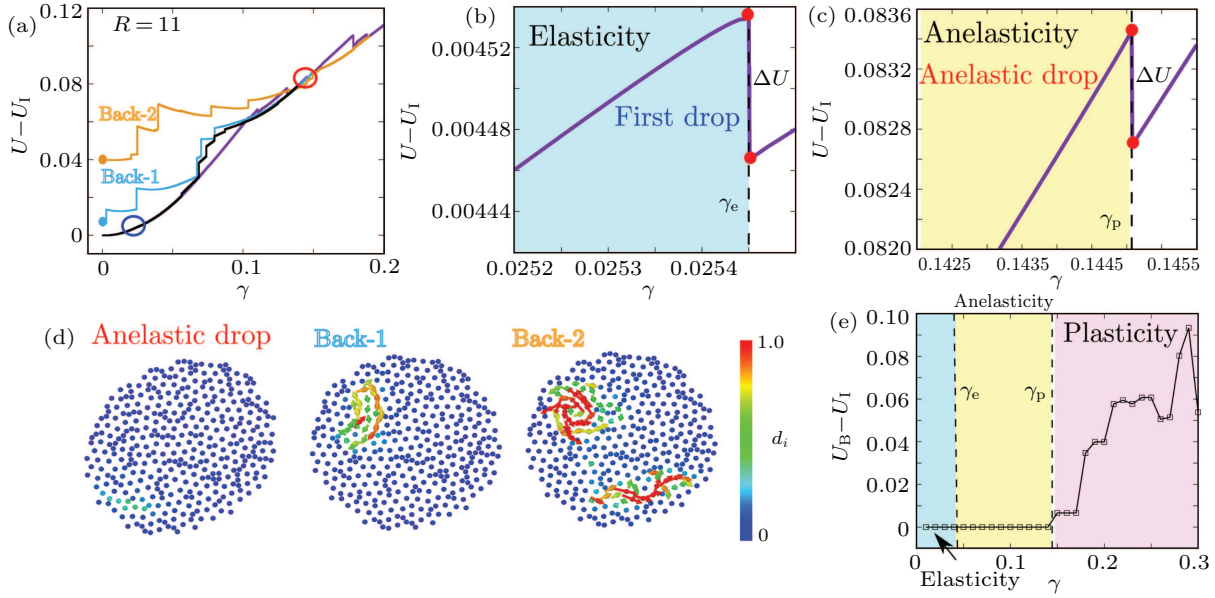


Fig. 3. The characterization of elastic, anelastic and plastic events by loading–unloading process. (a) The potential energy per atom (U) changes with strain during loading and unloading processes, where U_I is the potential energy per atom of the initial state. The purple curve shows the loading process, and the black one shows the anelastic unloading process, starting from a strain of $\gamma = 0.14$. The yellow and cyan unloading curves start from $\gamma = 0.15$ and 0.19, respectively, and back-1 and back-2 indicate the corresponding unloaded states. (b) The first drop event during the loading process, marked by a blue circle in (a), and the strain of the first drop event (γ_e), below which the unloading curve matches the loading curve. (c) The last anelastic drop event during the loading process, and the corresponding strain (γ_p), marked by a red circle in (a). (d) Depiction of atomic displacement in three sample scenarios: anelastic drops, back-1, and back-2. (e) Evolution of potential energy difference from the unloaded state to the initial state with loading strain. Three distinct regions are illustrated by γ_e and γ_p, indicated by the vertical dash line.

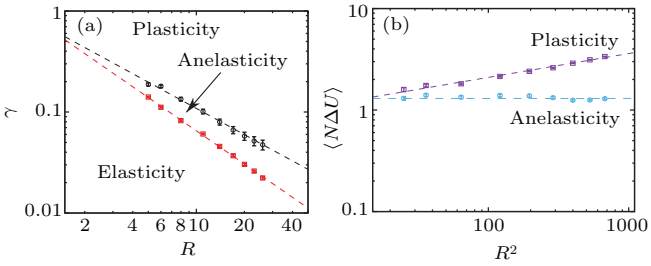


Fig. 4. (a) The strain boundaries of elasticity and anelasticity γ_e and of anelasticity and plasticity γ_p depend on system size R. (b) The mean value of avalanche size $N\Delta U$ for anelasticity and plasticity, respectively, varies with the square of the system size R^2.

The finite size exponent can determine the property of avalanche statistic, and the avalanche size is defined as $N\Delta U$. The boundary between anelasticity and plasticity is marked by γ_p. Avalanches during loading between γ_e and γ_p are anelastic; beyond this range, they are plastic. Figure 4(b) illustrates avalanche size statistics. Plastic avalanches grow with the system size, while anelastic ones stay constant regardless of the size. It reveals that the anelastic avalanche is a localized event, which is distinguished from the sub-extensitive nature of plastic avalanche.[12,13] The anelastic event can be recognized as the basin hopping within a metabasin based on the view of potential energy landscape,[24,40] and the accumulation of basin hopping would arouse metabasin hopping, it means that the plastic event can be only triggered when the strain is larger than γ_p. Therefore, the anelasticity can be identified as the activation of element excitation, such as STZ[10] or fluid units,[41] and the sub-extensitive plasticity is composed of the element excitation, and entangled with long range elasticity.

4. Conclusion

In summary, our study focused on understanding the transition from anelasticity to plasticity in amorphous solids. We employed molecular dynamics simulations using athermal quasistatic shear and frozen matrix methods. By analyzing various parameters, we identified three distinct deformation modes: elasticity, anelasticity, and plasticity. We found that anelasticity acts as a critical intermediary between elasticity and plasticity, and it precedes the onset of plastic deformation. The transition from anelasticity to plasticity is influenced by both the system size (R) and the applied loading strain (γ). We characterized this transition using key parameters γ_e and γ_p. The transition from anelasticity to plasticity occurs when the loading strain exceeds γ_p. Anelastic events were found to exhibit localized behavior, while plastic events exhibited subextensive behavior.

Our findings suggest that plasticity arises from the inter-

action of a series of anelastic events, with anelastic events acting as potential element excitations in amorphous solids. The transition from anelasticity to plasticity is influenced by system size and loading strain, and the properties of avalanche statistics depend on the system size and the distinction between anelastic and plastic avalanches.

Acknowledgements

Project supported by Guangdong Major Project of Basic and Applied Basic Research, China (Grant No. 2019B030302010), the National Natural Science Foundation of China (Grant No. 52130108), Guangdong Basic and Applied Basic Research, China (Grant No. 2021B1515140005), and Pearl River Talent Recruitment Program (Grant No. 2021QN02C04).

References

[1] Schuh C, Hufnagel T and Ramamurty U 2007 *Acta Mater.* **55** 4067
[2] Wang W H 2012 *Prog. Mater. Sci* **57** 487
[3] Hufnagel T, Schuh C and Falk M 2016 *Acta Mater.* **109** 375
[4] Cheng Y Q and Ma E 2011 *Prog. Mater. Sci* **56** 379
[5] Barrat J and Lemaitre A 2011 *Heterogeneities in amorphous systems under shear* (Oxford University Press) p. 246
[6] Nicolas A, Ferrero E, Martens K and Barrat J 2018 *Rev. Mod. Phys.***90** 045006
[7] Argon A 1979 *Acta Metallurgica* **27** 47
[8] Shi Y F and Falk M 2005 *Phys. Rev. Lett.* **95** 095502
[9] Schall P, Weitz D and Spaepen F 2007 *Science* **318** 1895
[10] Karmakar S, Lerner E and Procaccia I 2010 *Phys. Rev. E* **82** 055103
[11] Lin J and Zheng W 2017 *Phys. Rev. E* **96** 033002
[12] Lerner E and Procaccia I 2009 *Phys. Rev. E* **79** 066109
[13] Maloney C and Lemaitre A 2004 *Phys. Rev. Lett.* **93** 016001
[14] Krisponeit J, Pitikaris S, Avila K, Küchemann S, Krüger A and Samwer K 2014 *Nat. Commun.* **5** 3616
[15] Antonaglia J, Wright W, Gu X J, Byer R, Hufnagel T, LeBlanc M, Uhl J and Dahmen K 2014 *Phys. Rev. Lett.* **112** 155501
[16] Lagogianni A, Liu C, Martens K and Samwer K 2018 *Eur. Phys. J. B* **91** 104
[17] Shang B S, Rottler J, Guan P F and Barrat J 2019 *Phys. Rev. Lett.* **122** 105501
[18] Duan J, Wang Y J, Dai L H and Jiang M Q 2023 *Phys. Rev. Mater.* **7** 013601
[19] Argon A 2013 *Philos. Mag.* **93** 3795
[20] Xu B, Falk M, Li J F and Kong L T 2017 *Phys. Rev. B* **95** 144201
[21] Richard D, Ozawa M, Patinet S, Stanifer E, Shang B S, Ridout S, Xu B, Zhang G, Morse P, Barrat J, Berthier L, Falk M, Guan P F, Liu A, Martens K, Sastry S, Vandembroucq D, Lerner E and Manning M 2020 *Phys. Rev. Mater.* **4** 113609
[22] Ebrahem F, Bamer F and Markert B 2020 *Phys. Rev. E* **102** 033006
[23] Regev I, Weber J, Reichhardt C, Dahmen K and Lookman T 2015 *Nat. Commun.* **6** 8805
[24] Harmon J, Demetriou M, Johnson W and Samwer K 2007 *Phys. Rev. Lett.* **99** 135502
[25] Wang W H 2019 *Prog. Mater. Sci.* **106** 100561
[26] Costa M, Londoño J, Blatter A, Hariharan A, Gebert A, Carpenter M and Greer A 2023 *Acta Mater.* **244** 118551
[27] Tomida T and Egami T 1993 *Phys. Rev. B* **48** 3048
[28] Shang B S, Wang W H and Guan P F 2022 *Acta Mater.* **225** 117557
[29] Regev I, Lookman T and Reichhardt C 2013 *Phys. Rev. E* **88** 062401
[30] Fiocco D, Foffi G and Sastry S 2014 *Phys. Rev. Lett.* **112** 025702
[31] Barbot A, Lerbinger M, Hernandez-Garcia A, García-García R, Falk M, Vandembroucq D and Patinet S 2018 *Phys. Rev. E* **97** 033001
[32] Thompson A, Aktulga H, Berger R, Bolintineanu D, Brown W, Crozier P, in t Veld J, Kohlmeyer A, Moore S, Nguyen T, Shan R, Stevens M, Tranchida J, Trott C and Plimpton S 2022 *Computer Physics Communications* **271** 108171
[33] Stukowski A 2009 *Model. Simul. Mater. Sci. Eng.* **18** 015012
[34] Patinet S, Vandembroucq D and Falk M 2016 *Phys. Rev. Lett.* **117** 045501
[35] Mizuno H, Mossa S and Barrat J 2013 *Phys. Rev. E* **87** 042306
[36] Lerbinger M, Barbot A, Vandembroucq D and Patinet S 2022 *Phys. Rev. Lett.* **129** 195501
[37] Castellanos D, Roux S and Patinet S 2021 *Comptes Rendus. Physique* **22** 135
[38] Castellanos D, Roux S and Patinet S 2022 *Acta Mater.* **241** 118405
[39] Lemaitre A and Maloney C 2006 *J. Stat. Phys.* **123** 415
[40] Blank-Burian M and Heuer A 2018 *Phys. Rev. E* **98** 033002
[41] Wang Z and Wang W H 2018 *Natl. Sci. Rev.* **6** 304